frontiers | Frontiers in Materials

TYPE Original Research
PUBLISHED 07 September 2022
DOI 10.3389/fmats.2022.992351

OPEN ACCESS

EDITED BY
Monireh Kouhi,
Isfahan University of Medical Sciences, Iran

REVIEWED BY
Liping Tong,
Shenzhen Institutes of Advanced Technology (CAS), China
Mosab Kaseem,
Sejong University, South Korea

*CORRESPONDENCE
Jiang Chen,
jiangchen@fjmu.edu.cn

†These authors have contributed equally to this work

SPECIALTY SECTION
This article was submitted to Biomaterials, a section of the journal Frontiers in Materials

RECEIVED 12 July 2022
ACCEPTED 05 August 2022
PUBLISHED 07 September 2022

CITATION
Su J, Xing X, Lin Y, Gao Y, Xing Y, Xu Z and Chen J (2022), In vitro physicochemical and biological properties of titanium alloy, zirconia, polyetheretherketone, and carbon fiber-reinforced polyetheretherketone. *Front. Mater.* 9:992351. doi: 10.3389/fmats.2022.992351

In vitro physicochemical and biological properties of titanium alloy, zirconia, polyetheretherketone, and carbon fiber-reinforced polyetheretherketone

Jingjing Su[1,2,3†], Xiaojie Xing[1,2,3†], Yanjun Lin[3†], Yuerong Gao[2], Yifeng Xing[3], Zhiqiang Xu[4] and Jiang Chen[5*]

[1]Fujian Key Laboratory of Oral Diseases, School and Hospital of Stomatology, Fujian Medical University, Fuzhou, China, [2]Fujian Provincial Engineering Research Center of Oral Biomaterial, School and Hospital of Stomatology, Fujian Medical University, Fuzhou, China, [3]Stomatological Key Lab of Fujian College and University, School and Hospital of Stomatology, Fujian Medical University, Fuzhou, China, [4]Department of Stomatology, Affiliated Hospital of Putian University, Putian, China, [5]School and Hospital of Stomatology, Fujian Medical University, Fuzhou, China

Implant repair is a common means to restore the normal function of the hard tissues (bone or teeth). At present, the commonly and potentially used implant materials include titanium alloy (Ti), zirconia (Zr), polyetheretherketone (PEEK), and 30% carbon fiber reinforced PEEK (CFR-PEEK). This study compares their physicochemical and biological properties, including surface morphology, contact angle, nano hardness, elastic modulus, and the impact on the proliferation and osteogenic differentiation of bone marrow mesenchyml stem cell. Additionally, the differences in bacteria adhesion rates among materials were compared. CFR-PEEK had the highest contact angle, followed by PEEK, Zr, and Ti. Zr had the highest nano hardness and modulus of elasticity, followed by Ti, CRF-PEEK, and PEEK. There was no statistically significant difference in cytotoxicity among materials based on the liquid extract test. However, the relative cell proliferation rate on the surface of CFR-PEEK was slightly lower than that of Ti and Zr. Moreover, alkaline phosphatase activity, extracellular matrix mineralization, and osteogenic gene expression with the Ti and Zr materials were higher than with the PEEK and CFR-PEEK materials at Day 7, and Zr showed the highest osteogenic gene expression level among materials at Day 14. Ti had the greatest number of bacterial colonies that adhered to it, followed by Zr, CFR-PEEK, and PEEK. While the mechanical properties of PEEK and CFR-PEEK were closer to bone tissue and their anti-adhesion effect against bacteria was better than those of Ti and Zr, modification methods are needed to improve the osteogenic properties of these biopolymers.

KEYWORDS

implant materials, physicochemical properties, osteogenic differentiation, bacterial adhesion, cytotoxicity

1 Introduction

Orthopedic and dental implant restoration is a common technique for patients with bone loss caused by trauma, cancer, inflammation, and congenital abnormalities (Qin et al., 2019). While metals and ceramics are often used in this field, their application has limitations. Specifically, in terms of mechanical properties, the "stress shielding" effect is caused by the significant difference in elastic modulus between titanium (Ti, 110 GPa), zirconia (Zr, 210 GPa), and bone tissue (13–18 GPa), leading to peri-implant bone resorption and even implant loss (Mishra and Chowdhary, 2019; Knaus et al., 2020). In terms of biological properties, tiny metal particles can be released from the implant's surface, causing aseptic inflammatory reactions (Sadowsky, 2020). Although Ti is an inert metal, sensitization and corrosion reactions still exist, and metal artifact reduction also influences the presence of peri-implant tissue (Sivaraman et al., 2018). Moreover, the silver-grey metal abutment impacts the visual aesthetics of implant restoration in patients with a thin-scalloped gingival biotype (Bathala et al., 2019). While ceramic material has biocompatibility and aesthetic advantages, its application remains restricted by its low fracture toughness and high brittleness (Yan et al., 2018).

Recently, biopolymers have attracted significant attention due to their unique physicochemical and biological properties. Polyetheretherketone (PEEK) is a polymer with one ketone and two ether bonds in its main chain structure, approved by the US Food and Drug Administration (FDA) as an implant material in orthopedics, cardiac and maxillofacial surgery, and cranioplasty (Zhang et al., 2019). In dentistry, PEEK is broadly used in prosthetics, implants, and orthodontics due to its good biocompatibility and high stability (Ma and Tang, 2014; Knaus et al., 2020). In addition, PEEK has an elastic modulus comparable to natural bone, effectively avoiding "stress shielding." Moreover, PEEK's color palette can match those of the teeth, and it is easy to process due to its good ductility (Khurshid et al., 2020; da Cruz et al., 2021).

While the mechanical properties of PEEK cannot meet the mechanical demands of dental implants, its mechanical strength can be improved by adding carbon fiber (Yu et al., 2020). Studies have shown that 30% carbon fiber-reinforced PEEK (CFR-PEEK) has improved elastic modulus and tensile strength compared with PEEK, with values closer to bone tissue or dentin (Fabris et al., 2022). Indeed, when CFR-PEEK and Ti were assessed using the finite element method (FEM) after compressive loading tests, the compressive strength of CFR-PEEK (450 N) completely met masticatory function requirements, with a maximal occlusal force of 140–170 N for anterior teeth and 250–400 N for posterior teeth (Lee et al., 2012). The biocompatible CFRPEEK combines the advantages of PEEK and carbon fiber, making it a promising new implant material (Hahnel et al., 2015; Li et al., 2015).

The mechanical properties and osseointegration of implants are the critical factors for the long-term stability of implant restorations (Cheng et al., 2018; Wang et al., 2021). Implant failure is often associated with bacterial adhesion to the implant's surface and subsequent biofilm formation (Blanco et al., 2021). While the performance of these implant materials has been studied previously, the biological responses of cells and bacteria to these biomaterials remain unclear (Hahnel et al., 2015; Peng et al., 2021; Rozeik et al., 2022). Therefore, this is the first study to evaluate and compare the physicochemical and biological properties of four implant materials: Ti, Zr, PEEK, and CFR-PEEK. In addition, it examines their surface properties and mechanical strength, their effects on viability and osteogenic differentiation of bone marrow mesenchymal stem cells (BMSCs), and their anti-adhesive properties against *Staphylococcus aureus (S. aureus)* and *Porphyromonas gingivalis (P. gingivalis)*.

2 Materials and methods

2.1 Sample preparation

Four implant materials: Ti (Ti6Al4V; Falcontech; Wuxi City, China), Zr (Wieland; Ulm, Germany), PEEK (Gehr; Mannheim, Germany), and 30% CFR-PEEK (Roeching; Mannheim, Germany) were cut into disc specimens with a diameter of 10 ± 0.1 mm and thickness of 2 ± 0.1 mm, then highly polished with silicon carbide abrasive paper (240-600-800 grit), ultrasonically cleaned with acetone, ethanol, deionized water, and sterilized at 121°C for 30 min.

2.2 Surface characterization

2.2.1 Morphology and roughness

Thermal-field emission scanning electron microscope (FE-SEM; Magellan 400; Phoenix, AZ, United States) was used to observe material morphology. The materials were sprayed with gold under a vacuum for 60 s before observation. The arithmetic means deviation of the surface (Ra) was obtained with a probe contact profiler (SEF 680; Kosaka Laboratory Ltd; Tokyo, Japan) over a measuring length of 4.0 mm by sampling a length of 0.8 mm at a scanning speed of 1.0 mm/s.

2.2.2 Contact angle

Hydrophilicity was evaluated at room temperature (RT) using a contact angle analyzer (OCA20; Dataphysics; Filderstadt, Germany). The initial orientation of the deionized water droplet was perpendicular to the sample, and the contact angle of 3 μL deionized water on the sample surface was measured for 10 s.

2.2.3 Nano hardness and elastic modulus

We used an experimental nanoindentation NHT2 instrument (Anton Paar; Buchs, Switzerland) with a Berkovich-type indenter, a load resolution of 50 nN, and a displacement resolution of 0.01 nm. The experimental loading process was performed as follows: the load control mode was used, and a constant loading rate of 30 mN/min was applied throughout the loading process until the load reached a maximum of 15 mN. The maximal load was held for 10 s to avoid the creep effect, then unloaded at the same rate until the indenter was entirely disengaged, and five points were measured.

2.3 In vitro biological performance

2.3.1 Cell culture

BMSCs were isolated from the bone marrow of 4-week-old male Sprague-Dawley rats (SPF class; Shanghai Laboratory Animal Center [SLAC]; Shanghai, China). This project was reviewed and approved by the ethics committee of Fujian Medical University (FJMU-2021073; Fuzhou, China). BMSCs were cultured in a low sugar Dulbecco's modified Eagle's medium (DMEM; Hyclone; Logan, UT, United States) with 10% fetal bovine serum (FBS; Hyclone), and 1% penicillin and streptomycin antimycotic (Hyclone) in a constant temperature incubator (37°C, 5% CO_2). The culture medium was renewed every 3 days, and cells of the third to fifth generation were used in all experiments.

2.3.2 Cell morphology

BMSCs were inoculated onto material samples in 24-well plates at a density of 5×10^4/well. After incubation for 24 h, samples were transferred to a new 24-well plate, rinsed twice with phosphate-buffered saline (PBS), and cells were fixed with 2.5% glutaraldehyde overnight at 4°C. Then, the samples were dehydrated in a graded ethanol series (30, 50, 70, 80, 90, 100%) for 10 min, dried in a critical point dryer, sputter-coated with gold, and observed with SEM (SUPRA 55; Zeiss; Oberkochen, Germany).

2.3.3 Cytotoxicity evaluation with extract and direct contact test

The extracted liquid of the material samples was obtained according to ISO 10993-12: 2021 with the medium surface area/volume of 3 cm^2/ml and incubated at 37 °C for 24 h. The BMSCs were seeded into 96-well plates and onto the samples at a density of 4×10^3/well and 2×10^4/well, respectively. After culturing for 24 h, the culture medium was replaced with liquid extracts in the experimental group and a fresh culture medium in the control group. DMEM containing 10% cell counting kit (CCK)-8 solution (Dojindo; Kumamoto, Japan) was added to each well on days 1, 3, and 5, and the optical density (OD) at 450 nm was obtained using a spectrophotometer (SpectraMax iD3; Molecular Devices; San Jose, CA, United States). The equation used to calculate the relative growth rate (RGR) was: RGR = OD of experimental group/OD of negative control group × 100%. Cytotoxicity was evaluated according to the toxicity grading method of US Pharmacopoeia (USP XXII, NF XVII, 1990).

2.3.4 Alkaline phosphatase activity

The BMSCs were seeded onto samples in 24-well plates at a density of 5×10^4/well. After culturing for 24 h, the medium was removed and replaced with an osteogenic medium (DMEM with 10% FBS, 1% β-glycerophosphate, 1% vitamin C, and 0.01% dexamethasone), and culturing continued for an additional 7 days. Then, cells were stained for ALP with the 5-bromo-4-chloro-3-indolyl-phosphate (BCIP)/nitro blue tetrazolium (NBT) color development kit (Beyotime; Haimen, China), and the samples were observed under a stereomicroscope (Stemi 508; Zeiss). Quantitative determination was performed using an ALP assay kit (Beyotime), and the OD of each culture was measured at 520 nm. Total protein content was determined using a bicinchoninic acid (BCA) assay kit (Beyotime). ALP activity is presented as King unit/g total protein.

2.3.5 Extracellular matrix mineralization

Fourteen days after BMSC osteogenic induction, the samples were washed with PBS and fixed with 4% paraformaldehyde (PFA) for 15 min. Samples were stained with Alizarin Red dye (ARS; pH = 6.6; Solarbio; Beijing, China) for 10 min at RT and observed under a stereomicroscope. Then, the adsorbed alizarin red dyes were dissolved in 10 mm sodium phosphate (pH 7.0) with 10% cetylpyridinium chloride (Boc Sciences; Shirley, NY, United States), and their absorbance was measured at 562 nm.

2.3.6 Real-time quantitative reverse transcription PCR analysis

Osteogenic-related gene expression was quantified using RT-qPCR. BMSCs were seeded onto material samples at 5×10^4/well and cultured in the osteogenic medium for 7 days. Total RNA was extracted with the TRIZOL reagent (Takara; Kusatsu, Japan) and reversely transcribed into complementary DNA (cDNA) according to the manufacturer's protocols. The cDNA was used as a PCR template to quantify the expression of biomineralization associated alkaline phosphatase (*Alpl*), type 1 collagen (*Col1a1*), runt-related transcription factor 2 (*Runx2*), osteocalcin (*Bglap*), osteopontin (*Spp1*), bone sialoprotein (*Ibsp*), and glyceraldehyde 3-phosphate dehydrogenase (*Gapdh*). The primers used are listed in Table 1.

TABLE 1 Primer sequences used for RT-qPCR.

Gene	Forward primer sequence (5′-3′)	Reverse primer sequence (5′-3′)
Gapdh	ACGGCAAGTTCAACGGCACAG	GAAGACGCCAGTAGACTCCACGAC
Alpl	CGTTTTCACGTTTGGTGGCT	ACCGTCCACCACCTTGTAAC
Col1a1	CGAGTATGGAAGCGAAGGTT	CTTGAGGTTGCCAGTCTGTT
Runx2	CAGATTACAGATCCCAGGCAGAC	AGGTGGCAGTGTCATCATCTGAA
Bglap	AATAGACTCCGGCGCTACCT	ATAGATGCGCTTGTAGGCGT
Spp1	GAGCAGTCCAAGGAGTATAAGC	AACTCGTGGCTCTGATGTTC
Ibsp	ACAACACTGCGTATGAAACCTATGAC	AGTAATAATCCTGACCCTCGTAGCC

2.4 Antibacterial activity

2.4.1 Bacteria culture

A frozen strain of *S. aureus* (ATCC25923; American Type Culture Collection [ATCC]; Manassas, VA, United States) was revived by aerobic culturing in Luria-Bertani (LB) medium (Hopebio; Qingdao, China) for 24 h, and a frozen strain of *P. gingivalis* (ATCC33277; ATCC) was revived by anaerobic culturing in the brain-heart infusion broth medium (BHI; Oxoid; Basingstoke, UK) containing 5 mg/L of hemins, 1 mg/L of vitamin K3, and 5% yeast extract for 48 h. The concentration of bacterial liquid was adjusted to 1×10^8 colony forming units (CFU)/mL based on absorbance at 600 nm.

2.4.2 Bacteria morphology

The samples were co-incubated with 1 ml of bacterial suspension at 37°C for 24 h. After removing the liquid medium, samples were rinsed with PBS and fixed with 2.5% glutaraldehyde at 4°C overnight. Then, samples were dehydrated and dried for 10 min with 30, 50, 70, 80, 90, 95, and 100% ethanol. The morphology and numbers of bacteria on the surface of the samples were observed by scanning electron microscopy (QUANTA 450; Field Electron and Ion Company [FEI]; Hillsboro, OR, United States).

2.4.3 CFU counting

100 μL of *S. aureus and P. gingivalis* suspension with a concentration of 1×10^8 CFU/ml were dripped onto material samples, and 1 ml of medium was added to the wells. After culturing for 24 h, the medium was discarded, and samples were washed twice with PBS to remove non-adhered bacteria. Then, adhered bacteria were collected using a vortex mixer. Aliquots of the bacterial suspension were diluted with PBS to ratios of 1:10, 1:100, 1:1,000, and 1:10,000. Each dilution was evenly coated onto an agar plate. *S. aureus and P. gingivalis* colonies were counted according to *ISO 7218:2007* after culturing for 24 and 48 h, respectively.

2.5 Statistical analysis

All the data are presented as mean ± standard deviations. Data were tested for normality (Shapiro-Wilk normality test) and variance homogeneity (Brown-Forsythe test) and analyzed with one-way analysis of variance (ANOVA) using the GraphPad Prism 9.0 software (GraphPad Software Inc.; San Diego, CA, United States). The following symbols are used to denote statistical significance in the graphs: *, $p < 0.05$; **, $p < 0.01$; ***, $p < 0.005$.

3 Results

3.1 Surface characterization

The disc-shaped samples of the four different implant materials are shown in Figure 1A. Representative FE-SEM images show that Ti and Zr had fewer scratches than PEEK and CFR-PEEK (Figure 1B). All tested samples had a similar surface roughness with a Ra of ~1.0 μM (Table 2), with no significant differences among groups ($p > 0.05$). Zr showed the highest nanohardness and elastic modulus value, followed by Ti, CFR-PEEK, and PEEK. PEEK had a significantly larger contact angle than the Ti and Zr groups, and its nanohardness and elastic modulus improved significantly with the addition of carbon fibers (Figure 1C; Table 2). However, the inhomogeneous distribution of carbon fibers caused fluctuations in nanohardness (Figure 1D).

3.2 Cell morphology

The morphology of BMSCs adhered to the Ti, Zr, PEEK, and CFR-PEEK samples are shown in Figure 2A. The cell distribution on each material was relatively uniform. While cells on the Ti, Zr, and PEEK showed expanded shapes with obvious pseudopodia, those on CFR-PEEK were smaller, spindle-shaped, or triangular, with relatively few pseudopods.

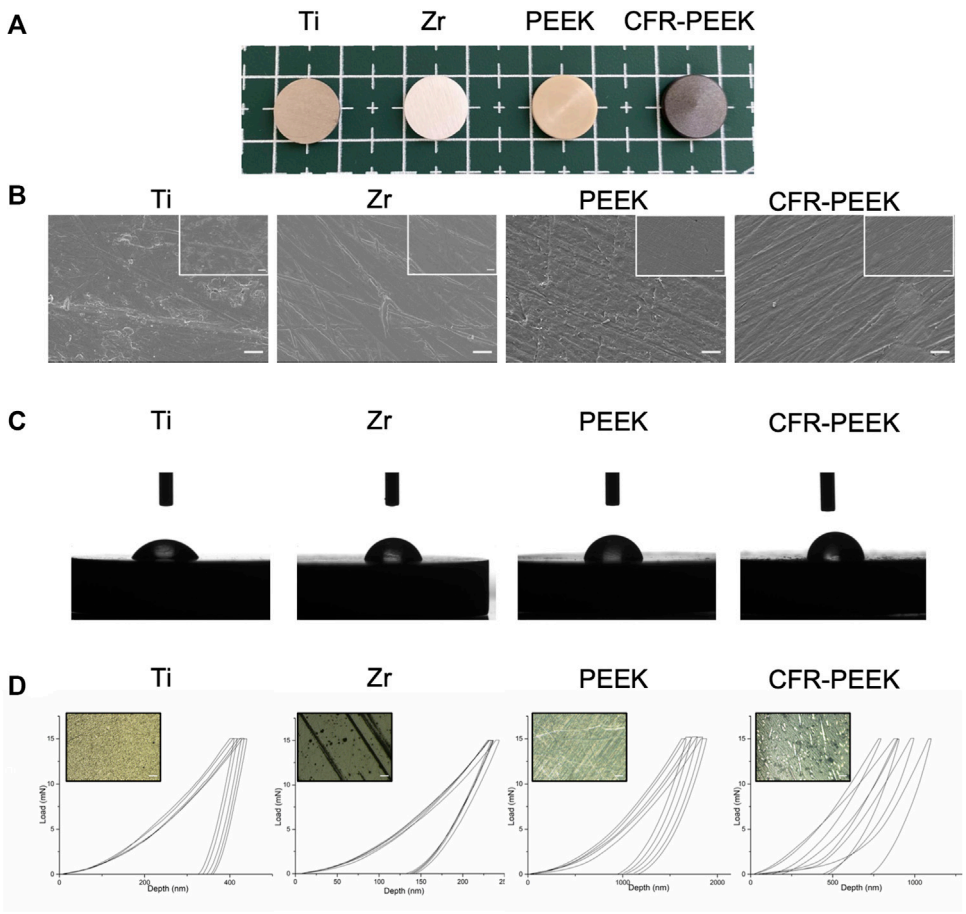

FIGURE 1
Surface characterization of four different implant materials. **(A)** Photographs of four different implant samples: Ti, Zr, PEEK, and CFR-PEEK. **(B)** FE-SEM images of Ti, Zr, PEEK, and CFR-PEEK samples under low and high magnifications (2000×, bar = 5 μM; 5,000×, bar = 2 μM). **(C)** The contact angle of different samples. **(D)** The load-displacement curves for different samples, where the upper-left image shows an optical microscope image (1,000×, bar = 10 μM) of the punctured area.

TABLE 2 Comparison of different materials (mean ± SD).

Group	Roughness (μm)	Contact angle (°)	Nano hardness (GPa)	Elastic modulus (GPa)
Ti	1.05 ± 0.07	65.68 ± 2.75	4.71 ± 0.27	133.17 ± 7.01
Zr	0.99 ± 0.04	77.36 ± 2.65	18.54 ± 0.19	250.50 ± 12.35
PEEK	1.04 ± 0.06	87.80 ± 4.70	0.29 ± 0.04	4.49 ± 0.25
CFR-PEEK	1.01 ± 0.06	97.75 ± 4.92	1.46 ± 0.70	13.20 ± 1.48

3.3 Cytotoxicity

Cytotoxicity did not differ significantly among groups at any time point ($p > 0.05$). The relative proliferation rates were all >95% in the liquid extract test (Figure 2B). In addition, there was no noticeable difference in BMSC proliferation rates on the Ti, Zr, and PEEK surfaces ($p > 0.05$; Figure 2C), while the rate on the CFR-PEEK surface was slightly lower than those of the Ti and Zr surfaces ($p < 0.05$) in the direct contact test.

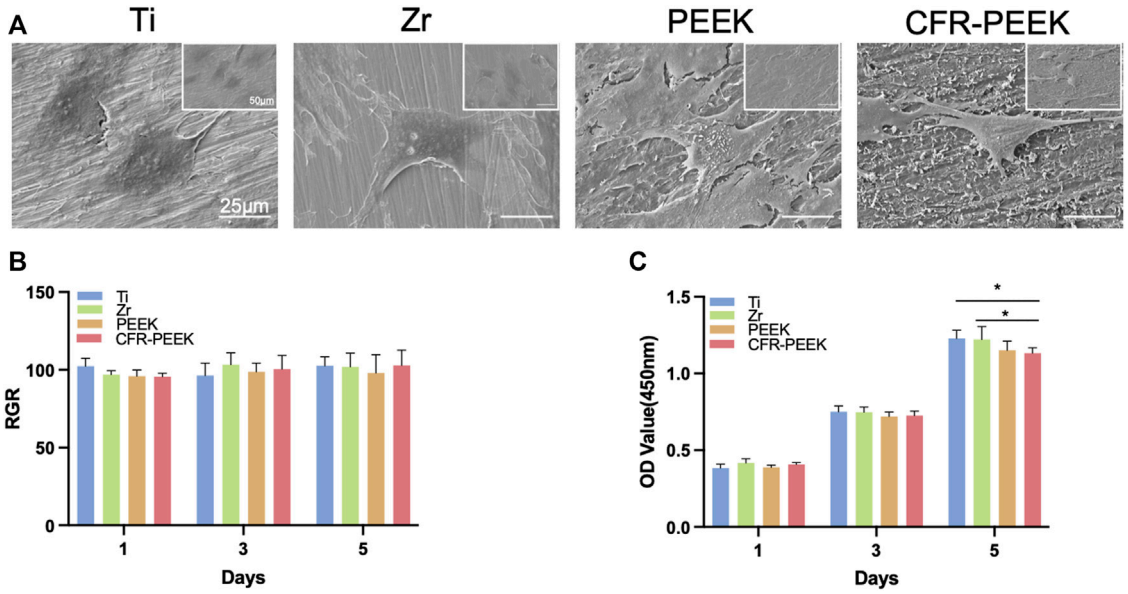

FIGURE 2
The morphology of BMSCs and cytotoxicity of four different implant materials. **(A)** SEM images of BMSCs adhered on Ti, Zr, PEEK, and CFR-PEEK materials at low and high magnifications (1,000×, bar = 25 μM; 500×, bar = 50 μM). **(B)** Cytotoxicity evaluation of the Ti, Zr, PEEK, and CFR-PEEK materials on days 1, 3, and 5 with the liquid extract test. **(C)** Cytotoxicity evaluation of the Ti, Zr, PEEK, and CFR-PEEK materials on days 1, 3, and 5 with the direct contact test. *$p < 0.05$.

3.4 ALP assay

The ALP staining images of BMSCs cultured on the different materials for 7 days are shown in Figure 3A. ALP activity was similar on Ti and Zr ($p > 0.05$), which were significantly higher than PEEK and CFR-PEEK ($p < 0.05$; Figure 3B).

3.5 ECM mineralization

The results of the ARS staining of BMSCs cultured on the different materials for 14 days are shown in Figure 3C. Zr had the greatest number of mineralization nodules, followed by Ti, PEEK, and CFR-PEEK, consistent with the quantitative analysis results (Figure 3D).

3.6 RT-qPCR

Relative gene expression levels in BMSCs cultured on the different materials for 7 and 14 days were shown in Figure 4. In the early stages of osteogenic differentiation, *Alpl* expression was consistent with the ALP activity assay. *Col1a1*, *Runx2*, and *Bglap* expression with Ti and Zr were significantly higher than with PEEK and CFR-PEEK (Figure 4A). Gene expression differences became more apparent among groups on day 14 (Figure 4B) and were highest with Zr.

3.7 Bacterial morphology and number

The morphology and the number of colonies of *S. aureus* and *P. gingivalis* adhered to Ti, Zr, PEEK, and CFR-PEEK are shown in Figure 5A. The morphology of *S. aureus* and *P. gingivalis* was typical of coccus and bacillus, respectively. The number of adhered bacteria was greatest with Ti, followed by Zr and CFR-PEEK, where bacteria were found in groups. A small number of bacteria was observed on PEEK, scattered across its surface.

3.8 CFU

The number of adhered *S. aureus* and *P. gingivalis* colonies was greatest on Ti, followed by Zr, CFR-PEEK, and PEEK ($p < 0.005$; Figures 5B–D).

4 Discussion

The surface and mechanical properties, biocompatibility, osteogenic ability, and antibacterial effect of four implant materials (Ti, Zr, PEEK, CFR-PEEK) were studied. The morphology, roughness, and wettability of biomaterials play essential roles in cell attachment and viability (Mehl et al., 2016). While PEEK and CFR-PEEK showed more textures

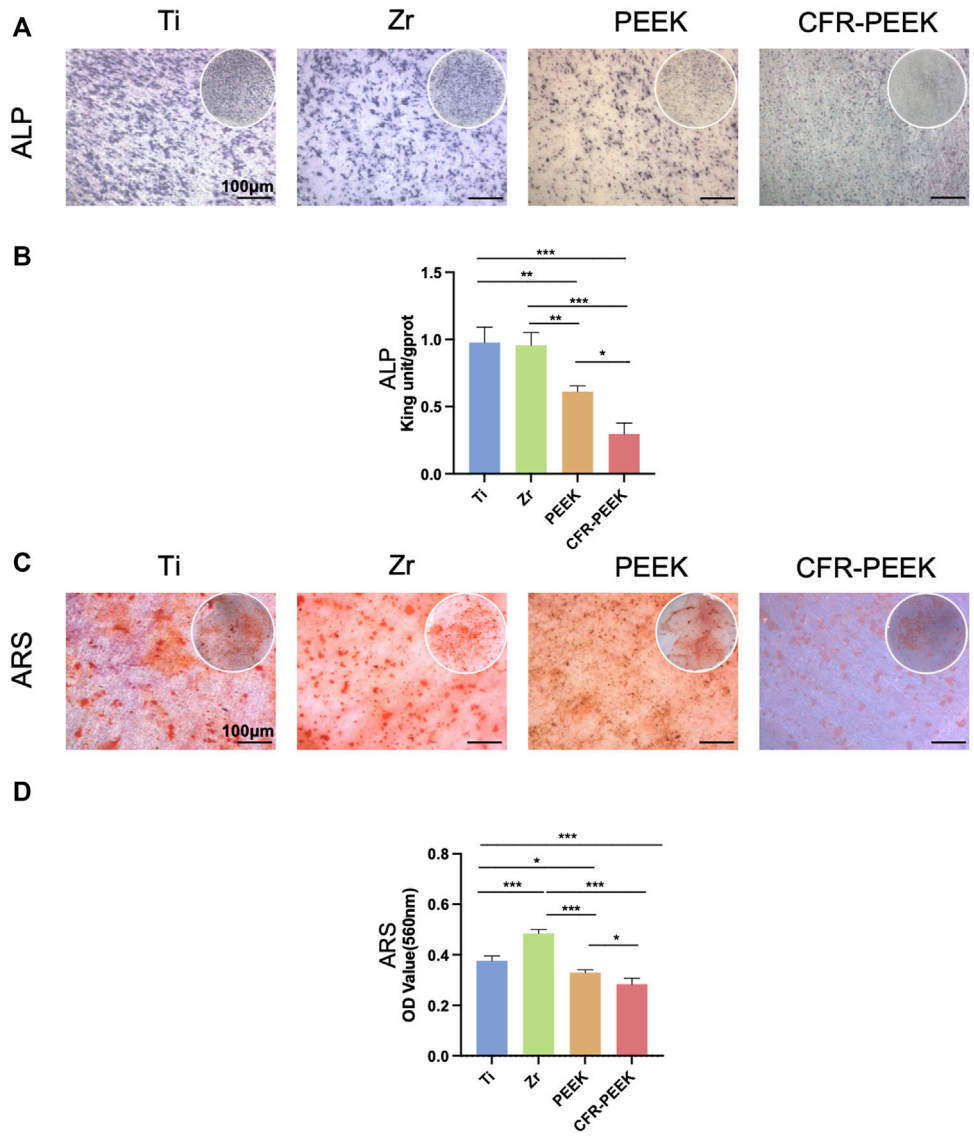

FIGURE 3
The ALP and ARS staining and quantification of four different implant materials. **(A)** ×25 magnification (bar = 100 μM) images of ALP staining of BMSCs cultured on Ti, Zr, PEEK, and CFR-PEEK for 7 days. **(B)** The quantitative ALP activity results of BMSCs on day 7. **(C)** Images of ARS staining of BMSCs cultured on the different materials for 14 days (25×, bar = 100 μM). **(D)** The quantitative ARS results for BMSCs on day 14. *$p < 0.05$; **$p < 0.01$; ***$p < 0.005$.

under SEM, there was no significant difference in the roughness among groups after polishing. The lower the water contact angle, the higher the material's hydrophilic properties (Lu et al., 2017). Ti showed the best wettability, followed by Zr, PEEK, and CFR-PEEK. This result may be due to the absence of polar functional groups on the surface of polymers (Peng et al., 2021). Moreover, the ideal mechanical property should benefit force distribution at the implant-bone interface (Ding et al., 2021), a suitable elastic modulus may promote the formation of new bone around the implant (Brizuela et al., 2019). Table 2 shows that the elastic modulus of PEEK (4.49 ± 0.25 GPa) and CFR-PEEK (13.20 ± 1.48 GPa) is closer to that of native bone tissue, which may avoid the stress shielding effect and enhance osseointegration (Fabris et al., 2022). Moreover, surface hardness is associated with resistance to force (Zhang et al., 2017). The hardness of trabecular and cortical bone lamellae in the human femur is between 0.234 and 0.760 GPa, which is close to that of alveolar bone (Zysset et al., 1999), and for native dentin is about 0.72 ± 0.10 GPa (Han et al., 2017). While the hardness of PEEK was significantly lower than Ti and Zr, it could be improved by the

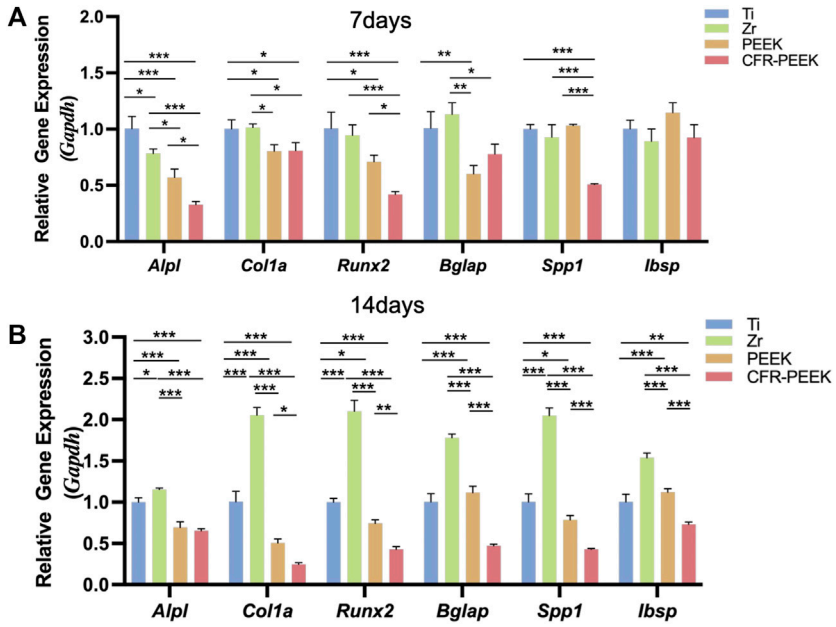

FIGURE 4
The osteogenic gene expression of four different implant materials. **(A)** The relative gene expression level of BMSCs cultured on Ti, Zr, PEEK, and CFR-PEEK for 7 days. **(B)** The relative gene expression level of BMSCs cultured on the different materials for 14 days. *$p < 0.05$; **$p < 0.01$; ***$p < 0.005$.

addition of carbon fiber, increasing to 1.46 ± 0.70 GPa for CFR-PEEK. Fabris et al. (2022) compared the tensile strength of PEEK and 30% CFR-PEEK, finding that the tensile strength of CFR-PEEK (217 MPa) was significantly higher than that of PEEK (115 MPa).

The morphology of BMSCs adhered to the surface of different materials was observed by SEM. The cells were evenly distributed and showed numerous filopodia with Ti, Zr, and PEEK, while CFR-PEEK showed weaker cell affinity, potentially related to its hydrophobicity (Jiao et al., 2021). Importantly, there were no significant differences in cytotoxicity among materials in the liquid extract test ($p > 0.05$), indicating good biocompatibility. However, the relative BMSC proliferation rate with CFR-PEEK first increased and then slightly decreased after 5 days in the direct contact test, but this reduction was not significant. There may be residues of nano-sized fiber debris resulting from the preparation of the carbon fibers, which adversely affects cell growth (Li et al., 2019). Qin et al. (2019) found a positive relationship between carbon fiber content and cytotoxicity. However, their long-term effects could be ignored.

This study evaluated the osteogenic differentiation of BMSCs cultured on the materials based on ALP activity, ARS staining, and qRT-PCR analysis. *Alpl*, *Col1a1*, and *Runx2* are primarily expressed in the early stages of osteoblasts differentiation, while mineralized nodules form, and *Bglap*, *Spp1*, and *Ibsp* are mainly expressed in the middle and late stages (Deng et al., 2015; Shalumon et al., 2018). The staining and RT-qPCR results showed that the osteogenic differentiation level with Ti and Zr was higher than with PEEK and CFR-PEEK on days 7 and 14.

Various surface properties, including morphology, hydrophilicity, and functional groups, influence the biological performance of biomaterials (Santoro et al., 2017). In previous studies, amorphous and smooth surfaces were more suitable for attachment and provided faster proliferation of osteoblast-like cells than highly crystalline surfaces (Sultana et al., 2017). PEEK and CFR-PEEK are semi-crystalline polymers containing both amorphous and crystalline phases owing to thermal processing, which may affect osteoblasts (Sagomonyants et al., 2008). Their hydrophilic surfaces also facilitate early blood contact, protein absorption, cell attachment, proliferation, differentiation, and bone regeneration (Hotchkiss et al., 2016). In this study, the CFR-PEEK was the most hydrophobic; water molecules could not form hydrogen bonds with the material's surface in the early stage, which is not conducive to protein adhesion in the later stage, leading to weak biological activity (Dubiel et al., 2011). High osteogenic gene expression with Zr on day 14 suggests that Zr could provide favorable conditions for cell mineralization (Lee et al., 2021). Based on the hydration and hydroxylation of surface oxide ions of Zr, abundant hydroxyl groups are believed to form on the surface, improving its wettability, facilitating cell adhesion, and enhancing bioactivity (Tamura et al., 2001; Zhao et al., 2014; Li et al., 2016).

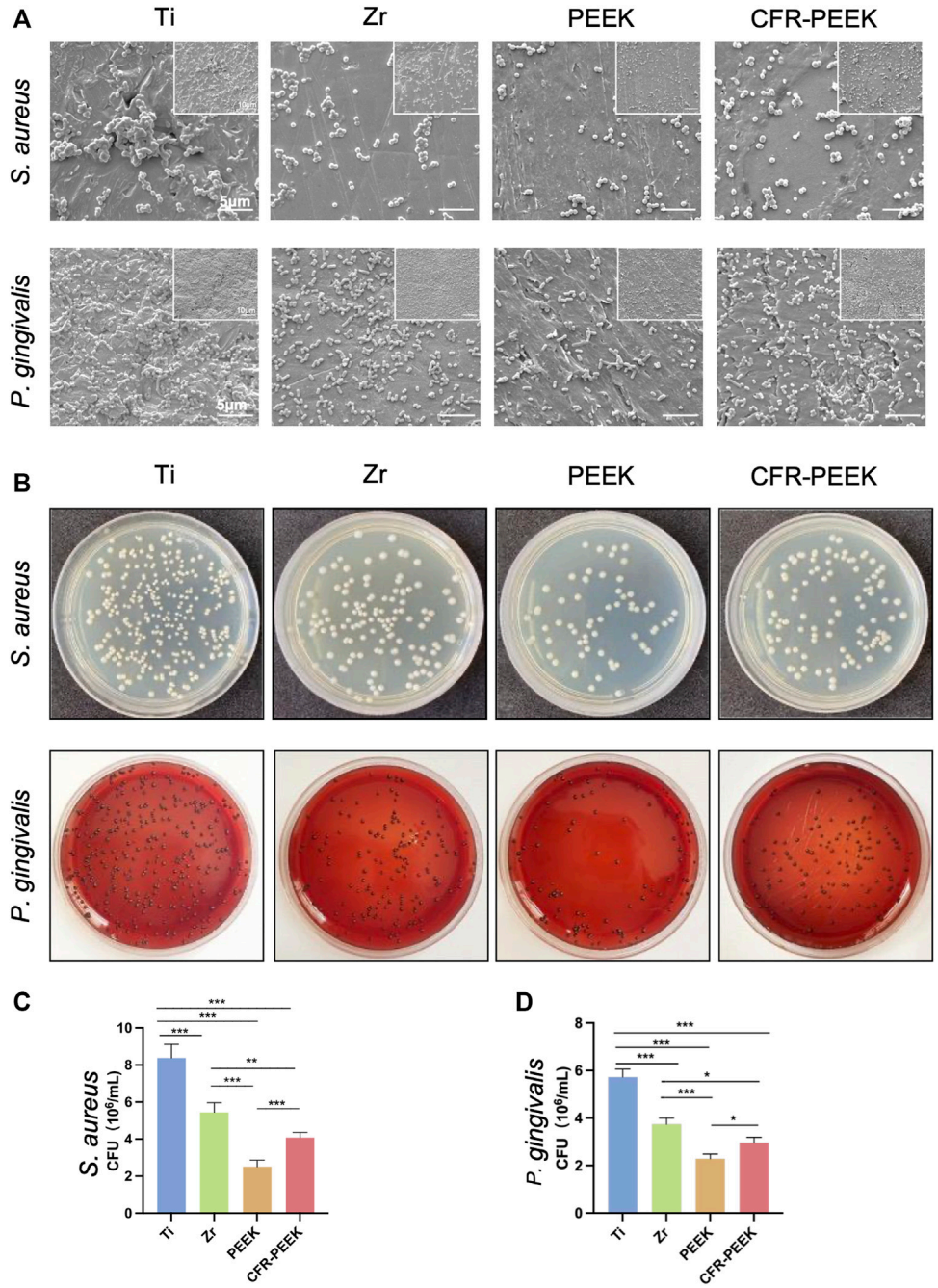

FIGURE 5
The anti-adhesion effect against bacteria of four different implant materials. **(A)** SEM images of bacterial morphology and the numbers of the colonies of *S. aureus* and *P. gingivalis* on Ti, Zr, PEEK, and CFR-PEEK samples under low and high magnifications (×10000, bar = 5 μM and 5,000×, bar = 10 μM). **(B)** The number of the colonies of *S. aureus and the P. gingivalis* cultured on agar. **(C)** The quantitative results of *S. aureus* colony counting. **(D)** The quantitative results of *P. gingivalis* colony counting. *$p < 0.05$, **$p < 0.01$, and ***$p < 0.005$.

While the osteogenic ability of PEEK and CFR-PEEK was significantly lower than that of Ti and Zr, many effective modifications were introduced to resolve this issue. For example, Zhang et al. (2022) developed a rough PEEK surface with a 200 nm patterned nanorod using a thermoforming technique, finding that this modification enhanced ALP activity and osteogenic gene expression in adipose stem cells and promoted the degree of peri-implant

neovascularization and osseointegration in rat femoral defect model. In addition, Guo et al. (2022) used the arc ion plating technique to apply a TiCu/TiCuN coating to CFR-PEEK, which showed excellent osteogenic activity *in vitro* and *in vivo*, as copper (Cu) could promote bone regeneration and antibacterial activity.

Gram-positive *S. aureus* and Gram-negative *P. gingivalis* have been associated with peri-implantitis (Persson and Renvert, 2014). The number of bacterial colonies on PEEK and CFR-PEEK was significantly lower than on Ti and Zr, consistent with Hahnel's findings (Hahnel et al., 2015). Biofilm formation on PEEK's surface was lower than on Ti and Zr, which may reflect differences in composition and morphology among materials (Qin et al., 2021). In addition, bacteria are more likely to adhere to the hydrophilic surface of Ti and Zr than PEEK (Malaikozhundan et al., 2016). Moreover, adding carbon fibers inhibited bacteria, possibly due to nanoscale carbon fragments and the "nano-blade" effect (Mei et al., 2020). The sharp edges of the nano-scaled sheets may destroy the integrity of bacterial membranes in physical contact (Malaikozhundan et al., 2016).

5 Conclusion

The new implant biocompatible materials PEEK and CFR-PEEK have comparable elastic modulus to native bone tissue and better bacterial anti-adhesion effects than Ti and Zr. However, the osteogenic ability of PEEK and CFR-PEEK still require improvement, and further studies are required to evaluate the effectiveness of different modification methods.

Data availability statement

The original contributions presented in the study are included in the article/supplementary material, further inquiries can be directed to the corresponding author.

Ethics statement

The animal study was reviewed and approved by the Affiliated Hospital of Fujian Medical University.

Author contributions

JS, XX, and YL contributed equally to this article. JS and XX: writing—original draft and editing. YL:writing—original draft, and formal analysis. YG: methodology, resources. YX: methodology, formal analysis. ZX: conceptualization. JC: conceptualization, supervision, project administration, funding acquisition.

Funding

This work was supported by the Joint Funds for the innovation of science and Technology of Fujian province (2019Y9031) and Startup Fund for scientific research, Fujian Medical University (2021QH2046).

Conflict of interest

The authors declare that the research was conducted in the absence of any commercial or financial relationships that could be construed as a potential conflict of interest.

Publisher's note

All claims expressed in this article are solely those of the authors and do not necessarily represent those of their affiliated organizations, or those of the publisher, the editors and the reviewers. Any product that may be evaluated in this article, or claim that may be made by its manufacturer, is not guaranteed or endorsed by the publisher.

References

Bathala, L., Majeti, V., Rachuri, N., Singh, N., and Gedela, S. (2019). The role of polyether ether ketone (peek) in dentistry - a review. *JMedLife.* 12 (1), 5–9. doi:10.25122/jml-2019-0003

Blanco, F. G., Hernández, N., Rivero-Buceta, V., Maestro, B., Sanz, J. M., Mato, A., et al. (2021). From residues to added-value bacterial biopolymers as nanomaterials for biomedical applications. *Nanomater. (Basel)* 11 (6), 1492. doi:10.3390/nano11061492

Brizuela, A., Herrero-Climent, M., Rios-Carrasco, E., Rios-Santos, J. V., Pérez, R. A., Manero, J. M., et al. (2019). Influence of the elastic modulus on the osseointegration of dental implants. *Mater. (Basel)* 12 (6), 980. doi:10.3390/ma12060980

Cheng, B. C., Koduri, S., Wing, C. A., Woolery, N., Cook, D. J., and Spiro, R. C. (2018). Porous titanium-coated polyetheretherketone implants exhibit an improved bone-implant interface: An *in vitro* and *in vivo* biochemical, biomechanical, and histological study. *Med. devices Auckl. N.Z).* 11, 391–402. doi:10.2147/mder.s180482

da Cruz, M. B., Marques, J. F., Peñarrieta-Juanito, G. M., Costa, M., Souza, J., Magini, R. S., et al. (2021). Bioactive-enhanced polyetheretherketone dental implant materials: Mechanical characterization and cellular responses. *J. Oral Implantol.* 47 (1), 9–17. doi:10.1563/aaid-joi-D-19-00172

Deng, Y., Zhou, P., Liu, X., Wang, L., Xiong, X., Tang, Z., et al. (2015). Preparation, characterization, cellular response and *in vivo* osseointegration of polyetheretherketone/nano-hydroxyapatite/carbon fiber ternary biocomposite. *Colloids Surfaces B Biointerfaces* 136, 64–73. doi:10.1016/j.colsurfb.2015.09.001

Ding, S. J., Chu, Y. H., and Chen, P. T. (2021). Mechanical biocompatibility, osteogenic activity, and antibacterial efficacy of calcium silicate-zirconia biocomposites. *ACS omega* 6 (10), 7106–7118. doi:10.1021/acsomega.1c00097

Dubiel, E. A., Martin, Y., and Vermette, P. (2011). Bridging the gap between physicochemistry and interpretation prevalent in cell-surface interactions. *Chem. Rev.* 111 (4), 2900–2936. doi:10.1021/cr9002598

Fabris, D., Moura, J., Fredel, M. C., Souza, J., Silva, F. S., and Henriques, B. (2022). Biomechanical analyses of one-piece dental implants composed of titanium, zirconia, PEEK, CFR-PEEK, or GFR-PEEK: Stresses, strains, and bone remodeling prediction by the finite element method. *J. Biomed. Mat. Res.* 110 (1), 79–88. doi:10.1002/jbm.b.34890

Guo, Y., Chen, C., Zhang, S., Ren, L., Zhao, Y., and Guo, W. (2022). Mediation of mechanically adapted TiCu/TiCuN/CFR-PEEK implants in vascular regeneration to promote bone repair *in vitro* and *in vivo*. *J. Orthop. Transl.* 33, 107–119. doi:10.1016/j.jot.2022.02.008

Hahnel, S., Wieser, A., Lang, R., and Rosentritt, M. (2015). Biofilm formation on the surface of modern implant abutment materials. *Clin. Oral Impl. Res.* 26 (11), 1297–1301. doi:10.1111/clr.12454

Han, M., Li, Q. L., Cao, Y., Fang, H., Xia, R., and Zhang, Z. H. (2017). *In vivo* remineralization of dentin using an agarose hydrogel biomimetic mineralization system. *Sci. Rep.* 7, 41955. doi:10.1038/srep41955

Hotchkiss, K. M., Reddy, G. B., Hyzy, S. L., Schwartz, Z., Boyan, B. D., and Olivares-Navarrete, R. (2016). Titanium surface characteristics, including topography and wettability, alter macrophage activation. *Acta Biomater.* 31, 425–434. doi:10.1016/j.actbio.2015.12.003

Jiao, J., Peng, C., Li, C., Qi, Z., Zhan, J., and Pan, S. (2021). Dual bio-active factors with adhesion function modified electrospun fibrous scaffold for skin wound and infections therapeutics. *Sci. Rep.* 11 (1), 457. doi:10.1038/s41598-020-80269-2

Khurshid, Z., Hafeji, S., Tekin, S., Habib, S. R., Ullah, R., Sefat, F., et al. (2020). "Titanium, zirconia, and polyetheretherketone (PEEK) as a dental implant material," in *Dental implants*. (Woodhead Publishing, Series), 5–35. doi:10.1016/B978-0-12-819586-4.00002-0

Knaus, J., Schaffarczyk, D., and Cölfen, H. (2020). On the future design of bio-inspired polyetheretherketone dental implants. *Macromol. Biosci.* 20 (1), e1900239. doi:10.1002/mabi.201900239

Lee, S. S., Huber, S., and Ferguson, S. J. (2021). Comprehensive *in vitro* comparison of cellular and osteogenic response to alternative biomaterials for spinal implants. *Mater. Sci. Eng. C* 127, 112251. doi:10.1016/j.msec.2021.112251

Lee, W. T., Koak, J. Y., Lim, Y. J., Kim, S. K., Kwon, H. B., and Kim, M. J. (2012). Stress shielding and fatigue limits of poly-ether-ether-ketone dental implants. *J. Biomed. Mat. Res.* 100 (4), 1044–1052. doi:10.1002/jbm.b.32669

Li, C. S., Vannabouathong, C., Sprague, S., and Bhandari, M. (2015). The use of carbon-fiber-reinforced (CFR) PEEK material in orthopedic implants: A systematic review. *Clin. Med. Insights Arthritis Musculoskelet. Disord.* 8, 33–45. doi:10.4137/CMAMD.S20354

Li, J., Qian, S., Ning, C., and Liu, X. (2016). rBMSC and bacterial responses to isoelastic carbon fiber-reinforced poly(ether-ether-ketone) modified by zirconium implantation. *J. Mat. Chem. B* 4 (1), 96–104. doi:10.1039/c5tb01784j

Li, Y., Wang, D., Qin, W., Jia, H., Wu, Y., Ma, J., et al. (2019). Mechanical properties, hemocompatibility, cytotoxicity and systemic toxicity of carbon fibers/poly(ether-ether-ketone) composites with different fiber lengths as orthopedic implants. *J. Biomaterials Sci. Polym. Ed.* 30 (18), 1709–1724. doi:10.1080/09205063.2019.1659711

Lu, H., Wang, J., Hao, H., and Wang, T. (2017). Magnetically separable MoS2/Fe3O4/nZVI nanocomposites for the treatment of wastewater containing Cr(VI) and 4-chlorophenol. *Nanomater. (Basel)* 7 (10), 303. doi:10.3390/nano7100303

Ma, R., and Tang, T. (2014). Current strategies to improve the bioactivity of PEEK. *Int. J. Mol. Sci.* 15 (4), 5426–5445. doi:10.3390/ijms15045426

Malaikozhundan, B., Vaseeharan, B., Vijayakumar, S., Sudhakaran, R., Gobi, N., and Shanthini, G. (2016). Antibacterial and antibiofilm assessment of Momordica charantia fruit extract coated silver nanoparticle. *Biocatal. Agric. Biotechnol.* 8, 189–196. doi:10.1016/j.bcab.2016.09.007

Mehl, C., Kern, M., Schütte, A. M., Kadem, L. F., and Selhuber-Unkel, C. (2016). Adhesion of living cells to abutment materials, dentin, and adhesive luting cement with different surface qualities. *Dent. Mat.* 32 (12), 1524–1535. doi:10.1016/j.dental.2016.09.006

Mei, L., Zhu, S., Yin, W., Chen, C., Nie, G., Gu, Z., et al. (2020). Two-dimensional nanomaterials beyond graphene for antibacterial applications: Current progress and future perspectives. *Theranostics* 10 (2), 757–781. doi:10.7150/thno.39701

Mishra, S., and Chowdhary, R. (2019). PEEK materials as an alternative to titanium in dental implants: A systematic review. *Clin. Implant Dent. Relat. Res.* 21 (1), 208–222. doi:10.1111/cid.12706

Peng, T. Y., Shih, Y. H., Hsia, S. M., Wang, T. H., Li, P. J., Lin, D. J., et al. (2021). *In vitro* assessment of the cell metabolic activity, cytotoxicity, cell attachment, and inflammatory reaction of human oral fibroblasts on polyetheretherketone (PEEK) implant-abutment. *Polym. (Basel)* 13 (17), 2995. doi:10.3390/polym13172995

Persson, G. R., and Renvert, S. (2014). Cluster of bacteria associated with peri-implantitis. *Clin. Implant Dent. Relat. Res.* 16 (6), 783–793. doi:10.1111/cid.12052

Qin, W., Li, Y., Ma, J., Liang, Q., and Tang, B. (2019). Mechanical properties and cytotoxicity of hierarchical carbon fiber-reinforced poly (ether-ether-ketone) composites used as implant materials. *J. Mech. Behav. Biomed. Mat.* 89, 227–233. doi:10.1016/j.jmbbm.2018.09.040

Qin, W., Ma, J., Liang, Q., Li, J., and Tang, B. (2021). Tribological, cytotoxicity and antibacterial properties of graphene oxide/carbon fibers/polyetheretherketone composite coatings on Ti-6Al-4V alloy as orthopedic/dental implants. *J. Mech. Behav. Biomed. Mat.* 122, 104659. doi:10.1016/j.jmbbm.2021.104659

Rozeik, A. S., Chaar, M. S., Sindt, S., Wille, S., Selhuber-Unkel, C., Kern, M., et al. (2022). Cellular properties of human gingival fibroblasts on novel and conventional implant-abutment materials. *Dent. Mat.* 38 (3), 540–548. doi:10.1016/j.dental.2021.12.139

Sadowsky, S. J. (2020). Has zirconia made a material difference in implant prosthodontics? A review. *Dent. Mat.* 36 (1), 1–8. doi:10.1016/j.dental.2019.08.100

Sagomonyants, K. B., Jarman-Smith, M. L., Devine, J. N., Aronow, M. S., and Gronowicz, G. A. (2008). The *in vitro* response of human osteoblasts to polyetheretherketone (PEEK) substrates compared to commercially pure titanium. *Biomaterials* 29 (11), 1563–1572. doi:10.1016/j.biomaterials.2007.12.001

Santoro, F., Zhao, W., Joubert, L. M., Duan, L., Schnitker, J., van de Burgt, Y., et al. (2017). Revealing the cell-material interface with nanometer resolution by focused ion beam/scanning electron microscopy. *ACS Nano* 11 (8), 8320–8328. doi:10.1021/acsnano.7b03494

Shalumon, K. T., Kuo, C. Y., Wong, C. B., Chien, Y. M., Chen, H. A., and Chen, J. P. (2018). Gelatin/nanohyroxyapatite cryogel embedded poly(lactic-co-glycolic acid)/nanohydroxyapatite microsphere hybrid scaffolds for simultaneous bone regeneration and load-bearing. *Polym. (Basel)* 10 (6), 620. doi:10.3390/polym10060620

Sivaraman, K., Chopra, A., Narayan, A. I., and Balakrishnan, D. (2018). Is zirconia a viable alternative to titanium for oral implant? A critical review. *J. Prosthodont. Res.* 62 (2), 121–133. doi:10.1016/j.jpor.2017.07.003

Sultana, T., Amirian, J., Park, C., Lee, S. J., and Lee, B. T. (2017). Preparation and characterization of polycaprolactone-polyethylene glycol methyl ether and polycaprolactone-chitosan electrospun mats potential for vascular tissue engineering. *J. Biomater. Appl.* 32 (5), 648–662. doi:10.1177/0885328217733849

Tamura, H., Mita, K., Tanaka, A., and Ito, M. (2001). Mechanism of hydroxylation of metal oxide surfaces. *J. Colloid Interface Sci.* 243 (1), 202–207. doi:10.1006/jcis.2001.7864

Wang, W., Qiao, S. C., Wu, X. B., Sun, B., Yang, J. G., Li, X., et al. (2021). Circ_0008542 in osteoblast exosomes promotes osteoclast-induced bone resorption through m6A methylation. *Cell Death Dis.* 12 (7), 628. doi:10.1038/s41419-021-03915-1

Yan, J. H., Wang, C. H., Li, K. W., Zhang, Q., Yang, M., Di-Wu, W. L., et al. (2018). Enhancement of surface bioactivity on carbon fiber-reinforced polyether ether ketone via graphene modification. *Int. J. Nanomedicine* 13, 3425–3440. doi:10.2147/IJN.S160030

Yu, W., Zhang, H., Yang, S., Zhang, J., Wang, H., Zhou, Z., et al. (2020). Enhanced bioactivity and osteogenic property of carbon fiber reinforced polyetheretherketone composites modified with amino groups. *Colloids Surf. B Biointerfaces* 193, 111098. doi:10.1016/j.colsurfb.2020.111098

Zhang, J., Tian, W., Chen, J., Yu, J., Zhang, J., and Chen, J. (2019). The application of polyetheretherketone (PEEK) implants in cranioplasty. *Brain Res. Bull.* 153, 143–149. doi:10.1016/j.brainresbull.2019.08.010

Zhang, S., Feng, Z., Hu, Y., Zhao, D., Guo, X., Du, F., et al. (2022). Endowing polyetheretherketone implants with osseointegration properties: *In situ* construction of patterned nanorod arrays. *Small* 18 (5), e2105589. doi:10.1002/smll.202105589

Zhang, Y., Chen, Y. Y., Huang, L., Chai, Z. G., Shen, L. J., and Xiao, Y. H. (2017). The antifungal effects and mechanical properties of silver bromide/cationic polymer nano-composite-modified Poly-methyl methacrylate-based dental resin. *Sci. Rep.* 7 (1), 1547. doi:10.1038/s41598-017-01686-4

Zhao, Y., Jamesh, M. I., Li, W. K., Wu, G., Wang, C., Zheng, Y., et al. (2014). Enhanced antimicrobial properties, cytocompatibility, and corrosion resistance of plasma-modified biodegradable magnesium alloys. *Acta Biomater.* 10 (1), 544–556. doi:10.1016/j.actbio.2013.10.012

Zysset, P. K., Guo, X. E., Hoffler, C. E., Moore, K. E., and Goldstein, S. A. (1999). Elastic modulus and hardness of cortical and trabecular bone lamellae measured by nanoindentation in the human femur. *J. Biomech.* 32 (10), 1005–1012. doi:10.1016/s0021-9290(99)00111-6